

vectors are only added during evaluation and do not permanently affect the design vectors \mathbf{x}_j in the current GA population. The time to produce each structure is proportional to N . For the L81 method each structure took about 5.5 days to produce (compare, 1.7 h for the NP method, where $N = 1$) on an SGI hardware platform running at 90 MHz. After each optimization $f_{95:300}$ for the best resulting design from each GA, denoted by \mathbf{x}_{opt} , was evaluated to measure accurately the expected perturbed performance. The results are shown in Fig. 2, where the changes in the average values of $f(\mathbf{x}_{\text{opt}})$, $f_{95}(\mathbf{x}_{\text{opt}})$, and the robustness r for each method are compared with the average performance of the 10 structures previously optimized using a nominal performance-only measure. r is a measure of the variability of the performance defined as

$$r(\mathbf{x}_{\text{opt}}) = |f_{95}(\mathbf{x}_{\text{opt}}) - f(\mathbf{x}_{\text{opt}})| \quad (5)$$

Depending on the specific aim of the optimization, either the worst level of f_{95} or r might be of primary concern.

The robust-optimal structures are not shown for brevity, but it is noted that all of the structures have irregular and different geometries of the nature shown in Fig. 1, and there is no apparent characteristic to identify the optimal from the robust-optimal structures.²

V. Results and Discussion

Optimizing for both robust and optimal structures has not compromised the average nominal performance but further improved it by up to 2 dB, except for the L81 method where there was a small degradation. On average, all methods improved f_{95} and the robustness by up to 3 and 4 dB, respectively. Although the GA using $f_{95:\text{OAT}}$ to estimate f_{95} had the best optimization performance, it has been shown that $f_{95:1.64}$ is the better estimator of f_{95} (Ref. 6). It is tentatively suggested that simply the use of geometric perturbations for GA optimization is more important for robust design than the precise details of the perturbations, especially as factor interactions were not considered.

In Fig. 3 the averaged results are normalized for the additional computational overhead for each method. It is seen that the success of the OAT method is achieved at the cost of a large increase in computational effort, whereas the NP2 method appears to provide improvements for little additional overhead. As the NP and NP2 methods require either no or double the computational effort, the consideration of robustness need not be expensive. It is, again tentatively, suggested that the NP and NP2 method are promising for efficient robust-optimal design using GAs of high-dimensional problems. There was no notable difference in the convergence speed between these two GAs.

Finally, it is noted that the damping ratio in the structure model (about 0.05 at 200 Hz) is higher than typically found in practice. Ongoing work on a practical three-dimensional structure suggests that this value could be 50 times too high.⁷ With less damping more sensitivity to geometric perturbations is expected, and a higher reward would be gained from considering robustness in the optimization.

VI. Conclusions

The work briefly presented here has demonstrated various schemes that can be incorporated into a genetic algorithm (GA) to help ensure that robust designs result from such search processes. They are all based on incorporating minor perturbations to the configurations evolved by the GA to assess their robustness. Of the methods considered, a series of one-at-a-time variations to the parameters being optimized yields the most robust designs but at high computational cost. A modified noisy phenotype method is shown to be almost as effective at ensuring robustness while being much more computationally efficient.

References

- Mitchell, M., *An Introduction to Genetic Algorithms*, MIT Press, Cambridge, MA, 1996.
- Anthony, D. K., Elliott, S. J., and Keane, A. J., "Robustness of Optimal Design Solutions to Reduce Vibration Transmission in a Lightweight 2-D Structure. Part I: Geometric Redesign," *Journal of Sound and Vibration*, Vol. 229, No. 3, 2000, pp. 505–528.

Vol. 229, No. 3, 2000, pp. 505–528.

³Taguchi, G., *System of Experimental Design*, UNIPUB/Kraus International Publications, New York, 1987.

⁴Tsutsui, S., and Ghosh, A., "Genetic Algorithms with a Robust Solution Searching Scheme," *IEEE Transactions on Evolutionary Computation*, Vol. 1, No. 3, 1997, pp. 201–208.

⁵Weismann, D., Hammel, U., and Bäck, T., "Robust Design of Multilayer Optical Coatings by Means of Evolutionary Algorithms," *IEEE Transactions on Evolutionary Computation*, Vol. 2, No. 4, 1998, pp. 162–167.

⁶Anthony, D. K., "Robust Optimal Design Using Passive and Active Methods of Vibration Control," Ph.D. Dissertation, Inst. of Sound and Vibration Research, Southampton Univ., Southampton, England, U.K., June 2000.

⁷Moshrefi-Torbati, M., Keane, A. J., Elliott, S. J., Brennan, M. J., and Rogers, E., "The Integration of Advanced Active and Passive Structural Vibration Control," *Proceedings of VETOMAC-I*, Indian Inst. of Science, Bangalore, India [CD-ROM], edited by K. Venkatraman and C. S. Manohar, 2000.

A. Messac
Associate Editor

Illustration of the Inclusion of Sound-Flow Interactions in Lighthill's Equation

Christophe Bogey,* Xavier Gloerfelt,†
and Christophe Bailly‡

Ecole Centrale de Lyon, 69134 Ecully, France

Introduction

LIGHTHILL'S equation¹ is an exact reformulation of the flow equations

$$\left(\frac{\partial^2}{\partial t^2} - c_0^2 \nabla^2 \right) \rho' = \frac{\partial^2 T_{ij}}{\partial x_i \partial x_j}(\mathbf{x}, t) \quad (1)$$

where $\rho' = \rho - \rho_0$ is the density fluctuation, ρ_0 and c_0 the ambient density and sound speed, and $T_{ij} = \rho u_i u_j + (p - c_0^2 \rho) \delta_{ij} - \tau_{ij}$ the Lighthill stress tensor, with u_i the velocity components, p the pressure, and τ_{ij} the viscous stresses. The classical interpretation of Eq. (1) consists of regarding the aerodynamic noise as solution of a wave equation in a fictitious medium at rest. The sound generation is assigned to the right-hand side, through the tensor T_{ij} , which is reduced to $T_{ij} = \rho u_i u_j$ in unheated flows at high Reynolds numbers. Thus, as long as T_{ij} is known, evaluated from the unsteady Reynolds averaged Navier-Stokes equations,² from large eddy simulation,³ or from direct numerical simulation,^{4,5} Eq. (1) can be solved for noise predictions.

Because Lighthill's equation is based on a wave equation in a medium at rest, the right-hand side contains both sound generation and flow effects on propagation. Two parts can actually be identified

Received 23 April 2002; revision received 4 September 2002; accepted for publication 16 September 2002. Copyright © 2003 by the authors. Published by the American Institute of Aeronautics and Astronautics, Inc., with permission. Copies of this paper may be made for personal or internal use, on condition that the copier pay the \$10.00 per-copy fee to the Copyright Clearance Center, Inc., 222 Rosewood Drive, Danvers, MA 01923; include the code 0001-1452/03 \$10.00 in correspondence with the CCC.

*Research Scientist, Laboratoire de Mécanique des Fluides et d'Acoustique, Unité Mixte de Recherche 5509 du Centre National de la Recherche Scientifique; christophe.bogey@ec-lyon.fr.

†Postdoctoral Student, Laboratoire de Mécanique des Fluides et d'Acoustique, Unité Mixte de Recherche 5509 du Centre National de la Recherche Scientifique.

‡Assistant Professor, Laboratoire de Mécanique des Fluides et d'Acoustique, Unité Mixte de Recherche 5509 du Centre National de la Recherche Scientifique. Member AIAA.

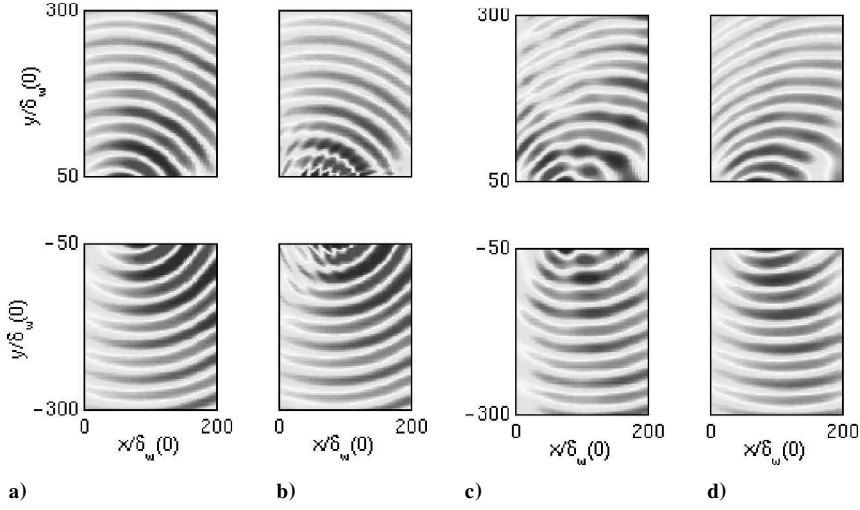


Fig. 1 Snapshots of the dilatation fields obtained at the same time: from Lighthill's equation using a) T_{ij}^f and c) T_{ij}^r ; b) from LEE without mean flow; and d) from Navier–Stokes equations. The dilatation scale is defined for levels from -1.5 to 1.5 s^{-1} .

in the Lighthill tensor: the terms quadratic in velocity fluctuations responsible for the noise generation by turbulence and the terms linear in acoustic fluctuations including flow–acoustic interactions. Then, for computing noise when flow effects on propagation are significant, the simulation providing T_{ij} must be compressible, and Eq. (1) must be integrated on the region encompassing all noise sources and sound–flow interactions. At this point, it should be noted that wave operators including some mean flow effects on propagation have been proposed, such as the third-order Lilley's wave operator⁶ for a unidirectional sheared mean flow or the linearized Euler equations (LEE) for general mean flows.⁷

The motivation of the present study is to illustrate the inclusion of sound–flow interactions in Lighthill's equation and to show that they can be taken into account provided that they are properly enclosed in the T_{ij} . It is a continuation of earlier works dealing with the accuracy of three-dimensional integral solutions of Lighthill's equation³ and with the hybrid method based on LEE developed by the authors.⁷ The flow involved in these two works is still considered in the present study because its sound field calculated directly from the Navier–Stokes equations is used as a reference solution. It is a mixing layer between two streams of velocity $U_1 = 0.12c_0$ and $U_2 = 0.48c_0$ in the lower and the upper parts, respectively. The flow, computed by large-scale simulation,³ is forced at discrete frequencies so that only the sound produced by the first vortex pairings is observed with a wavelength $\lambda_p = 51.5\delta_\omega(0)$ corresponding to the pairing period T_p , $\delta_\omega(0)$ being the initial vorticity thickness of the shear layer. Flow effects on sound propagation are important, and the Lighthill source region will enclose the shear flow for refraction⁸ and the acoustic domain for the convection by the two streams. Results obtained by solving Eq. (1) with the two-dimensional Green function will be compared to the reference solution and to a solution given by the LEE without mean flow for the propagation. The solution given by the LEE with the mean flow will not be used in this study because it is similar to the reference solution.⁷

Methodology

Two source terms are considered to study the different contributions of the Lighthill tensor: the first one, $T_{ij}^f = \rho u_i' u_j'$ with $u_i' = u_i - \bar{u}_i$ the velocity fluctuations, can be associated to the sound generation by the turbulence itself, and the second one, $T_{ij}^r = \rho u_i u_j$, is the full Lighthill tensor. They are recorded from the flow simulation every $T_p/11$ during $8 \times T_p$ on the whole computational domain defined by $0 \leq x_1 \leq 200\delta_\omega(0)$ and $-300\delta_\omega(0) \leq x_2 \leq 300\delta_\omega(0)$.

The time-domain solution of Eq. (1) in two dimensions is an infinite integral. Thus, in the present work, this equation is solved in the frequency domain.⁹ By applying the Fourier transform $\mathcal{F}[\phi(x, t)] = \hat{\phi}(x, \omega) = \int \phi(x, t) \exp(-i\omega t) dt$, an inhomogeneous

Helmholtz equation is derived from Eq. (1) for the angular frequency ω :

$$(\omega^2 + c_0^2 \nabla^2) \hat{\rho}'(x, \omega) = -\frac{\partial^2 \hat{T}_{ij}(x, \omega)}{\partial x_i \partial x_j} \quad (2)$$

The two-dimensional Green function associated to this equation is $\hat{G}(x|y, \omega) = (i/4c_0^2) H_0^{(2)}(\omega|x-y|/c_0)$, where $H_0^{(2)}$ is the Hankel function of the second kind and order zero. By convolving Eq. (2) with the Green function and applying the differential operator on \hat{G} , it yields

$$\hat{\rho}'(x, \omega) = -\int_{S(y)} \hat{T}_{ij}(y, \omega) \frac{\partial^2 \hat{G}}{\partial y_i \partial y_j}(x|y, \omega) dy$$

The acoustic field is calculated at the last recording time step. Snapshots of the fluctuating pressure $p' = c_0^2 \rho'$ are provided in a related AIAA Paper.¹⁰ However, in this short Note, dilatation $\Theta = \nabla \cdot \mathbf{u}$ is used to represent the sound field for the sake of the comparison with the reference solution. Dilatation is connected to the acoustic field by the relation $\Theta = -(1/\rho_0) \partial \rho' / \partial t$ in a medium at rest and by $\Theta = -(1/\rho_0) (\partial \rho' / \partial t + U_i \partial \rho' / \partial x_i)$ in a uniform flow of velocity U_i ($i = 1$ for the lower stream and $i = 2$ for the upper stream). The first relation is then applied to evaluate the dilatation when using T_{ij}^f in Lighthill's equation and the second one when using T_{ij}^r .

Results

The dilatation fields computed using T_{ij}^f and T_{ij}^r are displayed in Figs. 1a and 1c. They are strongly different in terms of wave front pattern and directivity. In Fig. 1a, waves fronts are circular and originate from the region of pairings near $x_1 = 70\delta_\omega(0)$. The directivity is well marked in the downstream direction. In Fig. 1c, waves fronts are significantly ovalized by the two uniform streams, and the directivity is pronounced for large angles.

The dilatation field of Fig. 1a, obtained from Lighthill's equation with T_{ij}^f , is compared to the dilatation field of Fig. 1b calculated by the hybrid method based on LEE without mean flow for the sound propagation.⁷ Wave fronts are in phase and have the same amplitude, and both directivities are well marked in the downstream direction. This good agreement is shown more quantitatively by the corresponding instantaneous dilatation profiles at $x = 130\delta_\omega(0)$ in Fig. 2a. This shows the equivalence of the two acoustic methods, namely Lighthill's equation with the reduced tensor T_{ij}^f and the LEE solved without mean flow. Both combine a wave operator in a medium at rest with nonlinear source terms corresponding only to a

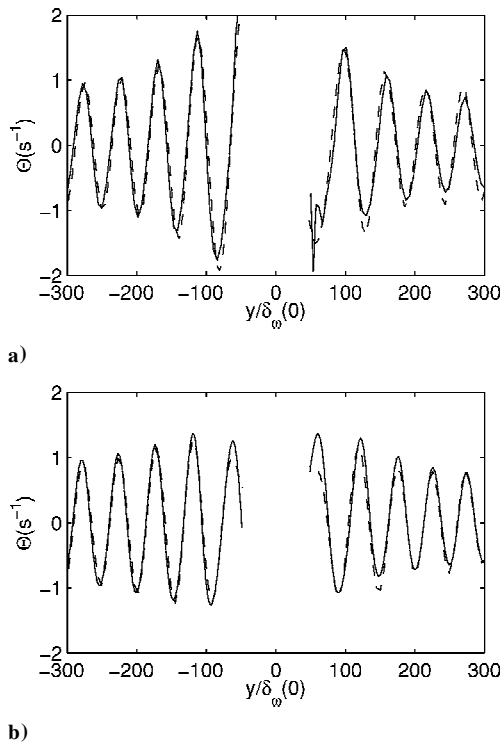


Fig. 2 Instantaneous dilatation profiles for $x = 130\delta_\omega(0)$, obtained at the same time as in Fig. 1: a) —, from LEE without mean flow and ---, from Lighthill's equation using T_{ij}^f ; and b) —, from Navier-Stokes equations and ---, from Lighthill's equation using T_{ij}^f .

sound generation problem, and therefore no sound-flow interaction is calculated.

The dilatation field of Fig. 1c, obtained from Lighthill's equation with T_{ij}^f , is now compared to the dilatation field of Fig. 1d computed directly by the flow simulation. Wave fronts are modified in the same way by the flow. Directivities are also affected similarly with preferred radiations for large angles from the downstream direction. The accordance is supported by Fig. 2b plotting the instantaneous dilatation profiles at $x = 130\delta_\omega(0)$. These profiles are located $60\delta_\omega(0)$ downstream the sound sources, in a region where wave fronts are significantly deformed by the flow. They superimpose fairly well with an agreement in phase and in amplitude. This demonstrates that flow effects on sound propagation are properly taken into account through the full Lighthill tensor, providing in this case both noise generation and sound-flow interactions.

Conclusions

The present application illustrates clearly that it is possible using Lighthill's equation to compute the noise radiated by a turbulent flow accounting for flow effects on sound propagation, provided that these sound-flow interactions are accurately included in the Lighthill tensor. This implies that the Lighthill tensor should be compressible and that it should be known on a region including all sound sources and all sound-flow interactions. Practically, it is difficult with the conventional flow simulation codes. Therefore, it is generally convenient to solve Lighthill's equation when flow effects on sound propagation are small but to use hybrid methods with wave operators including mean flow effects, such as Lilley's equation or the LEE, when these effects are significant.

References

- Lighthill, M. J., "On Sound Generated Aerodynamically—I. General Theory," *Proceedings of the Royal Society of London, Series A: Mathematical and Physical Science*, Vol. 211, No. 1107, 1952, pp. 564–587.
- Bastin, F., Lafon, P., and Candel, S., "Computation of Jet Mixing Noise Due to Coherent Structures: The Plane Jet Case," *Journal of Fluid Mechanics*, Vol. 335, 1997, pp. 261–304.
- Bogey, C., Bailly, C., and Juvé, D., "Numerical Simulation of the Sound

Generated by Vortex Pairing in a Mixing Layer," *AIAA Journal*, Vol. 38, No. 12, 2000, pp. 2210–2218.

⁴Mitchell, B. E., Lele, S. K., and Moin, P., "Direct Computation of the Sound Generated by Vortex Pairing in an Axisymmetric Jet," *Journal of Fluid Mechanics*, Vol. 383, 1999, pp. 113–142.

⁵Colonius, T., and Freund, J. B., "Application of Lighthill's Equation to a Mach 1.92 Turbulent Jet," *AIAA Journal*, Vol. 38, No. 2, 2000, pp. 368–370.

⁶Lilley, G. M., "The Generation and Radiation of Supersonic Jet Noise. Vol. IV—Theory of Turbulence Generated Jet Noise, Noise Radiation from Upstream Sources, and Combustion Noise. Part II: Generation of Sound in a Mixing Region," U.S. Air Force Aeropropulsion Lab., AFAPL-TR-72-53, Vol. 4, Wright-Patterson AFB, OH, 1972.

⁷Bogey, C., Bailly, C., and Juvé, D., "Computation of Flow Noise Using Source Terms in Linearized Euler's Equations," *AIAA Journal*, Vol. 40, No. 2, 2002, pp. 235–243.

⁸Rahier, G., and Redonnet, S., "Application de l'Équation de Lighthill au Calcul de Rayonnement Acoustique en Présence d'un Écoulement Non Uniforme," ONERA, RT 3/8020 DSNA/N, Châtillon, France, July 2000.

⁹Gloerfelt, X., Bailly, C., and Juvé, D., "Computation of the Noise Radiated by a Subsonic Cavity Using Direct Simulation and Acoustic Analogy," AIAA Paper 2001-2226, May 2001; also *Journal of Sound and Vibration* (to be published).

¹⁰Bogey, C., Bailly, C., and Juvé, D., "Noise Computation Using Lighthill's Equation with Inclusion of Mean Flow-Acoustics Interactions," AIAA Paper 2001-2255, May 2001.

W. J. Devenport
Associate Editor

Effect of Artificial Dissipation on Large-Eddy Simulation with Deconvolution Modeling

R. von Kaenel*

ETH Zürich, CH-8092 Zürich, Switzerland

N. A. Adams†

Technical University of Dresden,
D-01062 Dresden, Germany

L. Kleiser‡

ETH Zürich, CH-8092 Zürich, Switzerland

and

J. B. Vos§

CFS Engineering SA, CH-1015 Lausanne, Switzerland

Introduction

THE growing need in industrial computational-fluid-dynamics applications for accurate prediction of complex flows, for which Reynolds-averaged Navier–Stokes computations show unsatisfactory results, has led to the development of large-eddy simulation (LES) and new subgrid-scale models. In LES the Navier–Stokes equations are convolved with a smoothing filter, which reduces the numerical resolution requirement at the expense of a subgrid-scale model that represents the resolved-scale/nonrepresented-scale interaction. These subgrid-scale models often present a high level of

Received 29 August 2002; revision received 20 February 2003; accepted for publication 20 February 2003. Copyright © 2003 by the authors. Published by the American Institute of Aeronautics and Astronautics, Inc., with permission. Copies of this paper may be made for personal or internal use, on condition that the copier pay the \$10.00 per-copy fee to the Copyright Clearance Center, Inc., 222 Rosewood Drive, Danvers, MA 01923; include the code 0001-1452/03 \$10.00 in correspondence with the CCC.

*Ph.D. Student, Institute of Fluid Dynamics, Sonneggstrasse 3; vonkaenel@ifd.mavt.ethz.ch.

†Professor, Institute of Fluid Mechanics, George-Bähr Str. 3c.

‡Professor, Institute of Fluid Dynamics, Sonneggstrasse 3. Member AIAA.

§Senior Research Scientist, PSE-B.